



PERGAMON

Journal of the Mechanics and Physics of Solids
48 (2000) 709–734

JOURNAL OF THE
MECHANICS AND
PHYSICS OF SOLIDS

www.elsevier.com/locate/jmps

The influence of imperfections on the nucleation and propagation of buckling driven delaminations

J.W. Hutchinson^{a,*}, M.Y. He^b, A.G. Evans^a

^a*Division of Engineering and Applied Sciences, Harvard University, Cambridge, MA 02138, USA*

^b*Materials Department, University of California, Santa Barbara, CA 93106, USA*

Received 17 March 1999; received in revised form 5 July 1999

Abstract

The influence of prototypical imperfections on the nucleation and propagation stages of delamination of compressed thin films has been analyzed. Energy release rates for separations that develop from imperfections have been calculated. These demonstrate two characteristic quantities: a peak that governs nucleation and a minimum that controls propagation and failure. These quantities lead to two separate criteria that both need to be satisfied to cause failure. They involve a critical film thickness for nucleation and a critical imperfection wavelength for buckling. Implications for the avoidance of failure are discussed. © 2000 Elsevier Science Ltd. All rights reserved.

Keywords: A. Buckling; Crack propagation and arrest; Fracture toughness; B. Coatings; Films; C. Finite elements; Stability and bifurcation

1. Introduction

Compression in a film on a substrate can arise during the deposition process or due to temperature change when there is thermal expansion mismatch, or due to a combination of the two. Ceramic films or coatings on metal substrates will

* Corresponding author. Tel.: +1-617-495-2848; fax: +1-617-495-9837.

E-mail address: hutchinson@husm.harvard.edu (J.W. Hutchinson).

generally be in compression at room temperature if the film is deposited at high temperature. Oxidation and thermal barrier coatings are important examples receiving attention at the present time. These are multilayer systems consisting of at least one fully dense oxide layer (e.g. Al_2O_3) grown at high temperature on a bond coating applied to the metal alloy substrate. The oxide layer is subject to very large compressive stress when the system is cooled. Various failure modes have been observed, but one of the most common is cracking at the oxide/bond coat interface leading to buckling delamination and spalling.

Two competing failure mechanisms have been documented for compressed thin films (Evans and Hutchinson, 1995; Gioia and Ortiz, 1997; Hutchinson and Suo, 1992; Hutchinson et al., 1992; Nilsson and Giannakopoulos, 1995; Thouless et al., 1994; Wang and Evans, 1998). They comprise edge and buckle driven delamination (Fig. 1). In this paper the emphasis will be on buckling delaminations, but in this Section results for edge-delamination will be cited as background to understand the primary issue of the initial flaw size needed to nucleate failures. Films subject to an equi-biaxial compressive stress state, σ_0 , will be considered. When thermal expansion misfit is responsible for the residual compression, with a thick substrate having a higher coefficient of thermal expansion than the film, $\Delta\alpha > 0$, σ_0 is given by

$$\sigma_0 = E\Delta\alpha\Delta T/(1 - \nu) \quad (1)$$

when ΔT is drop in temperature from the state where the film is stress-free. Here, and throughout, E and ν are the Young's modulus and Poisson's ratio of the film. The elastic energy per unit area stored in the attached film is $(1-\nu)h\sigma^2/E$, where h is the film thickness. The energy per unit area which becomes available when the film is released from the substrate in a way such that it is still subject to a constraint of in-plane plane strain is

$$G_0 = \frac{(1 - \nu^2)h\sigma_0^2}{2E} \quad (2)$$

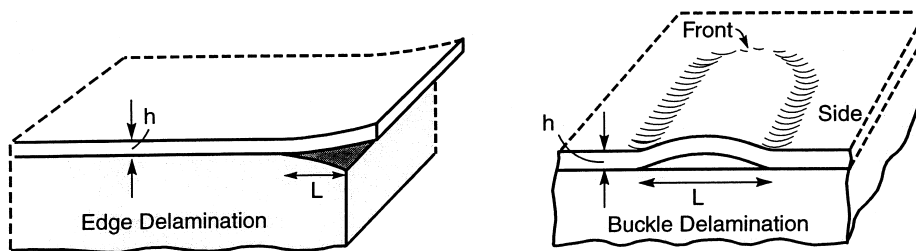


Fig. 1. Two prevalent delamination mechanisms for compressed films and coatings: edge delamination and buckledriven delamination. The buckle delamination is shown spreading from an edge to reveal the separation, but in most instances they initiate in the interior of the film away from any edges.

It will be seen that G_0 figures prominently in the energy release rates for both edge and buckle delaminations.

1.1. Edge delaminations

An initial edge flaw in the interface between film and substrate of sufficient magnitude can serve to nucleate an edge delamination which spreads as a plane strain interface crack (Fig. 1). For a film in compression, the interface crack is in mode II such that the faces remain in contact behind the advancing tip (Hutchinson and Suo, 1992). Under the idealized assumption that frictional sliding plays a negligible role, the steady-state energy release rate of the crack when its length is several times the film thickness is given by Eq. (1): i.e. $G = G_0$. Thus, if the mode II toughness of the interface is Γ_i^{II} (measured in units of energy per unit area), then the critical combination of film stress and thickness at which the edge-delamination can spread without arrest is

$$\sigma_0 = \sqrt{\frac{2E\Gamma_i^{II}}{(1 - \nu^2)h}} \tag{3}$$

Any frictional interaction of the crack faces will consume some of the energy stored in the film, and therefore Eq. (3) is necessarily an underestimate of the critical stress or film thickness.

The size of the interface edge flaws needed to nucleate a propagating edge-delamination are relatively small, generally on the order of several film thicknesses. This point is revisited after the size of flaws needed to initiate buckling delaminations has been discussed.

1.2. Buckling delamination

A buckling index is conveniently defined as

$$\Pi = (1 - \nu^2)(\sigma_0/E)(L/h)^2 \tag{4}$$

Throughout the paper both plane strain and axisymmetric delaminations will be considered to show that the behavioral features of interest are common to both. It will be convenient to let L denote both the width of the separation in plane strain and the diameter of a separation for axisymmetric geometries. For buckling to initiate Π must exceed a critical value Π_c . For a plane strain buckle, $\Pi_c = \pi^2/3 = 3.29$, and for a circular buckle, $\Pi_c = 4.89$. The buckling condition may be re-expressed in terms of the width or diameter of the delamination L_b at the onset of buckling. This is accomplished upon equating L to L_b and Π to Π_c in Eq. (4), such that

$$L_b/h = 1.81\sqrt{\bar{E}/\sigma_0} \text{ (plane strain)} = 2.21\sqrt{\bar{E}/\sigma_0} \text{ (axisymmetric)} \tag{5}$$

where \bar{E} is the plane strain modulus of the film, $\bar{E} = E/(1-\nu^2)$. These lengths represent the smallest interface separations which give rise to buckling delaminations absent any imperfections. For typical moduli and film compression levels, L_b will be about $20h$ or more. These relatively large interface flaws motivate the present investigation into the role of imperfections on the nucleation of buckling delaminations.

Energy release rates, G , and mode mixities, $\psi = \tan^{-1}(K_{II}, K_I)$ (where K_I and K_{II} are the mode I and II interface stress intensity factors), have been determined for plane strain and circular buckle delaminations by Hutchinson and Suo (1992) and Hutchinson et al. (1992). Plots of G/G_0 and ψ as a function of L/L_b are presented in Fig. 2 for circular delaminations. The energy release rate increases as the buckle spreads to sizes larger than L_b , while the relative proportion of mode II to mode I increases sharply.

The mode-dependence of the interface toughness $\Gamma_i(\psi)$ plays a critical role in determining the sequence of events in the propagation of the delamination. The following phenomenological interface toughness is adopted to model the dependence (Hutchinson et al., 1992)

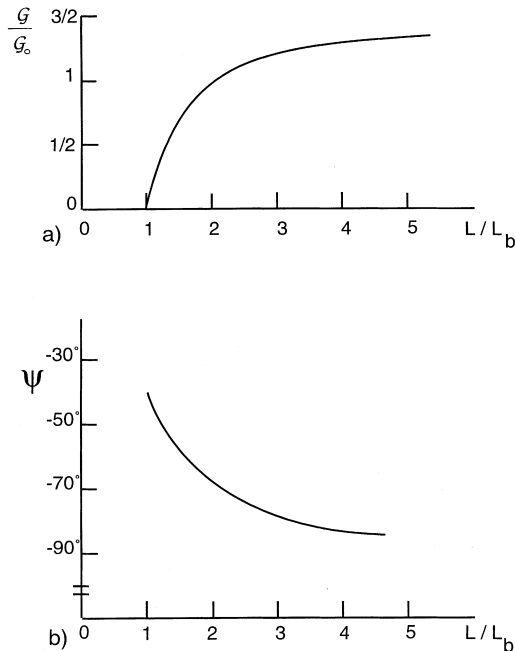


Fig. 2. Normalized energy release rate and mode mixity at the interface crack edge for circular delaminations of diameter L . For a given pre-compression σ_0 , L_b defined in Eq. (5) is the smallest diameter for which the film will buckle in the absence of an imperfection. ($\nu = 1/3$ and no elastic mismatch between film and substrate in the determination of ψ .)

$$\Gamma_i/\Gamma_i^I = 1 + \tan^2(1 - \lambda)\psi \tag{6}$$

where Γ_i^I is the mode I toughness and λ is a mixity index lying between 0 and 1. The interface toughness is mode independent in the limit $\lambda=1$. Representative values of λ for metal–ceramic interfaces generally have $\lambda < 0.3$. The criterion for the buckle delamination to grow is $G=\Gamma_i(\psi)$, which can be implemented using the results for G and ψ from Fig. 2 along with Eq. (6). Curves along which the criterion is satisfied for circular delaminations are plotted in Fig. 3 for four values of λ . The corresponding curves for plane strain delaminations are qualitatively similar. The curves may be interpreted in the following way. Suppose an initial separation of diameter L_0 exists at the interface, and let the compressive stress in the film, σ_0 , increase from zero. Two trajectories prior to propagation are illustrated as dashed curves emanating from the origin in Fig. 3, with the one connecting to A having a smaller L_0 than that connecting to B . (Note that on the dashed trajectories, $L/L_b \equiv L_0/L_b$ increases from zero because of the dependence of L_b on σ_0 in Eq. (5).) The condition for propagation is met when the dashed trajectory intersects the solid curve, which in Fig. 3 is illustrated for $\lambda=0$. If the intersection occurs on a falling portion of the curve, as in the case at A , any perturbed growth of the delamination will result in a state lying above the propagation criterion such that advance will occur dynamically at fixed stress until it arrests at A' . It will then grow stably under increasing stress. For larger initial separations, represented by the intersection at B , the advance is stable from the start with the delamination growing under increasing stress. Experimental observations and measurements have fully confirmed the two types of delamination growth: for a model system of mica bonded to an aluminum

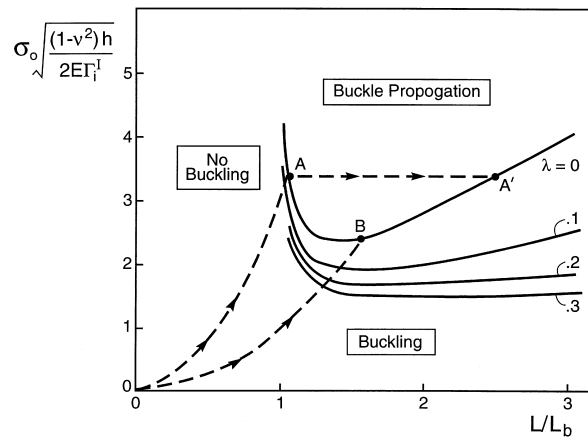


Fig. 3. A buckling map for a compressed film absent imperfections, with an initial separation, diameter L , at the interface. The sequence of steps in the delamination process are described in the text. ($\nu=1/3$ and no elastic mismatch between film and substrate in the determination of ψ .)

substrate (Hutchinson et al., 1992) and for a thermally grown oxide film (Al_2O_3) on a Ni superalloy substrate with a bond coat (Wang and Evans, 2000).

The limitation at this level of analysis is that the failure process cannot be activated until an interface separation has formed large enough to cause buckling (namely, $L_0 \geq L_b$). As already noted this requires, typically, $L_0 \approx 20 h$. Mechanisms responsible for creating separations this large have not been addressed, except in a qualitative manner for thermal barrier coating systems (Christensen et al., 1997; Evans et al., 1998; He et al., 1998; Wang and Evans, 1998, 2000). The intent of this article is to establish some of the mechanics relevant to this *nucleation stage of failure*. One consequence will be a modified buckling map that incorporates nucleation and more fully represents the buckling behavior found in practice. At this point it is also instructive to note from Eq. (2) that the energy required to drive a steady-state edge delamination is comparable to that for buckling delamination. Moreover, the size of an initial interface separation at the edge needed to initiate a propagating edge delamination is much smaller than $20 h$. The question naturally arises as to why edge delaminations are far less commonly observed as failure modes of compressed films than buckle delaminations. Part of the answer undoubtedly lies in the fact that edge delaminations are controlled by the mode II interface toughness (cf Eq. (3)) and must overcome frictional effects, if present. Although unresolved, the issue highlights the importance of understanding how interface separations much smaller than $20 h$ must in some way be able to nucleate buckle delaminations.

Two prototypical imperfections responsible for nucleation of interface separations in thermal barrier coatings have been proposed in the references cited above (Fig. 4): undulations and morphological heterogeneities. Both have the underlying feature that they locally redistribute the residual stress such that tensions develop normal to the interface (Evans et al., 1998; He et al., 1998), as illustrated in Fig. 4. These tensions provide the motivation for interface separations to nucleate and propagate. An analogous nucleation mechanism exists at the interface between particles in ceramic matrices driven by thermal expansion mismatch (e.g. Ito et al., 1981).

It has been possible to observe these processes in thermally grown thin films of $\alpha\text{-Al}_2\text{O}_3$ (TGO) formed on Ni-based bond coat alloys, because of the translucency of the oxide and the large reflectivity changes where the interface separates (Christensen et al., 1997; Tolpygo and Clarke, 1998; Wang and Evans, 1998, 2000). However, a mechanics analysis of this phenomenon and its implications for buckling delamination have yet to be provided. The intent of this article is to develop such an analysis and to use the results to establish the characteristics of imperfections that nucleate separations large enough to induce buckling and failure. Such results identify a *critical imperfection size* needed to activate the failure process.

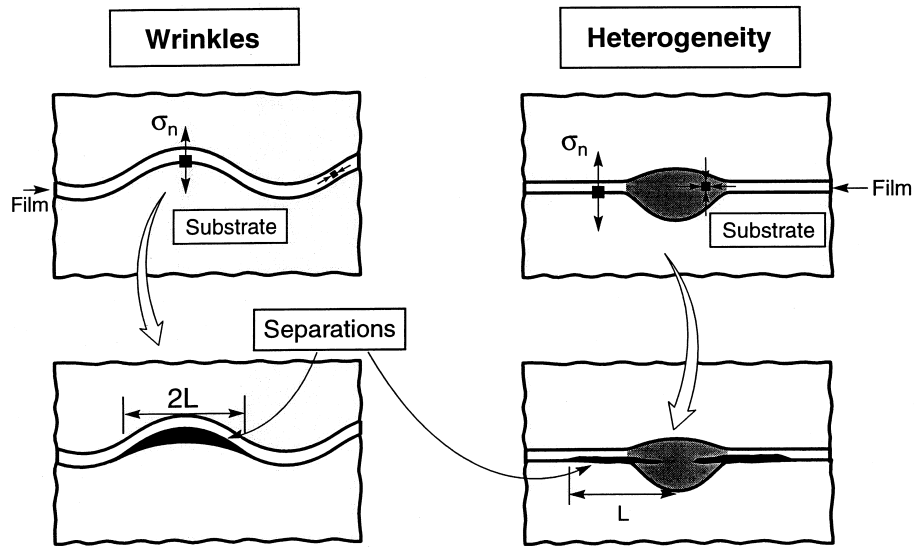


Fig. 4. Two types of imperfections that nucleate interface separations at the interface between the dense ceramic layer (usually a form of Al_2O_3) and the metallic bond coating in multilayer thermal barrier coatings.

2. Basic concepts

2.1. Role of imperfections

Previous analyses of interface separations emanating from imperfections (Evans, 1972; Evans et al., 1998; Rühle et al., 1987; Green, 1982; He et al., 1998; Ito et al., 1981; Shum and Huang, 1990) have revealed that, absent buckling, the energy release rate G exhibits a peak G_{peak} and thereafter asymptotically approaches zero (Fig. 5). Specific results are presented in Section 4. The consequence is that small flaws located near the regions of greatest tension can be activated, resulting in cracks that “pop-in” and arrest. Their size is governed by the declining portion of the energy release rate, with arrest occurring where G becomes coincident with the fracture toughness, Γ_i . This is the behavior identified on Fig. 5 as the *nucleation phase* of film failure.

As the separation becomes longer, it reaches a size large enough to buckle ($L \cong L_b$). When this happens, the energy release rate increases again, and approaches a value on the order of G_0 . This is the behavior identified on Fig. 5 as the *propagation phase*. Specific results are presented in Section 4.

The convolution of the opposing trends in G for nucleation and propagation results in a minimum, designated G_{min} . This minimum is one of the predominant

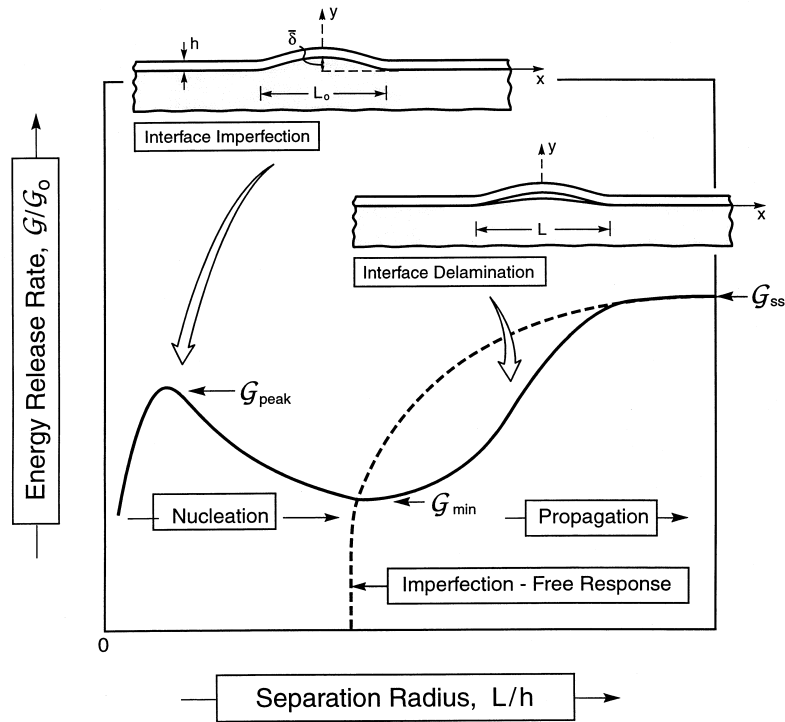


Fig. 5. A schematic of variations in energy release rate with separation width or diameter for the nucleation and propagation phases of failure. The critical quantities G_{\min} and G_{peak} are identified.

features governing film failure. Once G_{\min} attains Γ_i , the buckle propagates and reaches a size readily observable by optical microscopy.¹

One objective is to characterize G_{\min} and to explore its potential as a failure criterion for compressed thin films. A second is to establish trends in G_{peak} relevant to nucleation.

2.2. Buckling at imperfections

The influence of imperfections on film buckling is addressed at two levels. Analytical results are presented for a two-dimensional geometry, subject to plane strain. The localized imperfections are in the form of undulations having characteristic widths much smaller than the size of a buckled delamination (Fig.

¹ The subsequent approach to failure is dictated by effects of mode mixity and interface friction, discussed elsewhere (e.g. Wang and Evans, 1998).

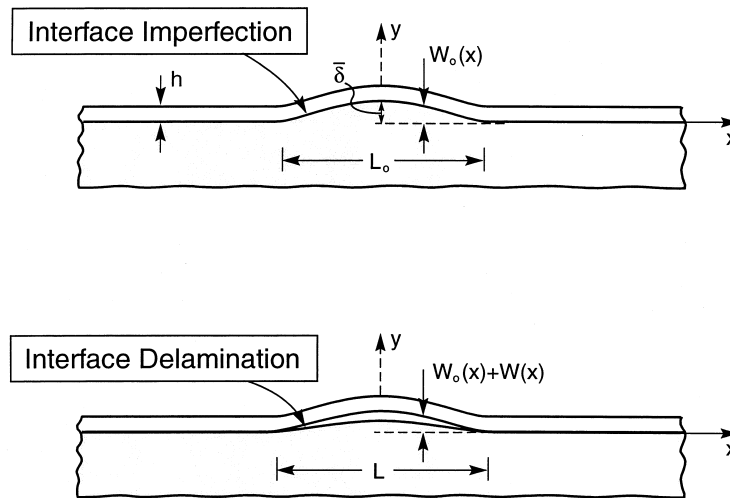


Fig. 6. A schematic of the undulation imperfection considered in the present analysis.

6). Corresponding results for axisymmetric buckles are analyzed numerically, using key insights from the analytical formulae both to establish the scope and to provide scaling relationships.

For the plane strain problem, the undulation, $w_0(x)$, is taken to be symmetric about $x = 0$. The film is otherwise uniform. Under restrictions that the maximum slope of the undulation should not exceed about 20° and that the film thickness is small compared with the delamination width, the von Karman nonlinear plate equations incorporating the imperfection can be used to describe the behavior of the delaminated film. These equations are equivalent to the nonlinear shallow shell equations (Koiter, 1966). They apply both when the delamination is too small to buckle (whereupon propagation is driven by the undulation), as well as when the debonded region is large enough to experience buckling driven delamination. Under the same conditions required for applicability of the Karman equations, the prestress in the attached film due to thermal expansion mismatch can be taken to be uniform and independent of the imperfection amplitude.²

The imperfection produces tensile stresses acting across the interface at points where w_0'' is negative. It is these stresses which promote imperfection-driven delamination (Fig. 4). As the delamination spreads into regions where w_0'' is positive, the compressive stress across the interface retards interface crack propagation, diminishing the energy release rate significantly (Fig. 5).

With the width of the delamination as L , the governing equations for $|x| \leq L/2$

² Neglecting terms of order $w_0'^2$ compared to unity.

can be reduced to the following system:

$$Dw'' + \sigma hw = -\sigma hw_0 + M^A \quad (7)$$

$$\sigma = \sigma_0 - \frac{\bar{E}}{L} \int_0^{L/2} (w'^2 + 2w_0'w') dx \quad (8)$$

where $(\)' = d(\)/dx$, $\bar{E} = E/(1-\nu^2)$, $D = \bar{E}h^3/12$. The term

$$M^A \equiv Dw''(L/2) + \sigma hw_0(L/2) \quad (9)$$

is an unknown quantity to be determined as part of the solution. The average stress in the x -direction in the detached film, σ , is independent of x . It is determined by condition (8) which has been obtained from the requirement that the component of displacement in the x -direction is zero at the end of the delamination. The boundary conditions accompanying Eqs. (7) and (8) are the symmetry condition at $x = 0$ and the clamped condition at $x = L/2$:

$$w'(0) = 0, \quad w(L/2) = 0, \quad w'(L/2) = 0 \quad (10)$$

The imperfection used in most of the numerical studies comprises a single wave having the shape (Fig. 6):

$$w_0 = \frac{\bar{\delta}}{2} \left(1 + \cos \frac{2\pi x}{L_0} \right) \quad |x| \leq \frac{L_0}{2}$$

$$= 0 \quad |x| \geq \frac{L_0}{2} \quad (11)$$

Application of the von Karman equations requires that the maximum slope of the imperfection not exceed about 1/5, limiting the amplitude of the imperfection to approximately $\bar{\delta} \leq L_0/10$. A family of extended imperfections (Fig. 7) illustrates barriers to delamination spreading:

$$w_0 = \frac{\bar{\delta}}{2} \left(1 + \cos \frac{2\pi x}{L_0} \right) e^{-(x/L_D)^2} \quad (12)$$

where L_D is a decay length illustrated on Fig. 7.

The two quantities determining the propagation of the interface crack are G and ψ . These are determined from the solution to the governing equations using (Hutchinson and Suo, 1992):

$$G = \frac{h}{2E} [(\sigma_0 - \sigma)^2 + 12(M(L/2)/h^2)^2] \quad (13)$$

$$\tan \psi = \frac{\sqrt{12}(M(L/2)/h^2) + (\sigma_0 - \sigma) \tan \omega}{-\sqrt{12}(M(L/2)/h^2) \tan \omega + (\sigma_0 - \sigma)} \tag{14}$$

where $M(L/2) = Dw''(L/2)$ is the moment at the right end of the delamination. Elastic mismatch between the film and substrate has some influence on the mode mixity, through ω . Here, the second Dundurs' mismatch parameter has been taken to be zero. The dependence of ω on the first parameter, $\alpha_D = (\bar{E} - \bar{E}_s) / (\bar{E} + \bar{E}_s)$, is specified in Hutchinson and Suo (1992). When there is no mismatch, $\omega = 52.1^\circ$.

For the single wave imperfection, Eq. (11), Eqs. (7) and (10) can be solved in closed form, with σ as an unknown variable. Then Eq. (8) can be reduced to a single algebraic transcendental equation for σ , completing the solution. The resulting equation for σ must be solved numerically for each set of parameters, except in some special instances. Then, G and ψ are evaluated using Eqs. (13) and (14).

For extended imperfections, Eq. (12), Eq. (7) requires numerical integration in addition to a numerical solution procedure for σ . Further details are given in Appendix A.

In the following Sections, the preceding formulae are used to analyze various effects of imperfections on plane strain buckling and buckle propagation. Corresponding results for axisymmetric buckles are determined numerically. For this purpose, axisymmetric separations are introduced at the interface and the energy release rate, G , as well as mode mixity angle, ψ , calculated as a function of the separation diameter, L , using procedures described elsewhere (Evans et al., 1998; He et al., 1998). The commercial finite element code ABAQUS was

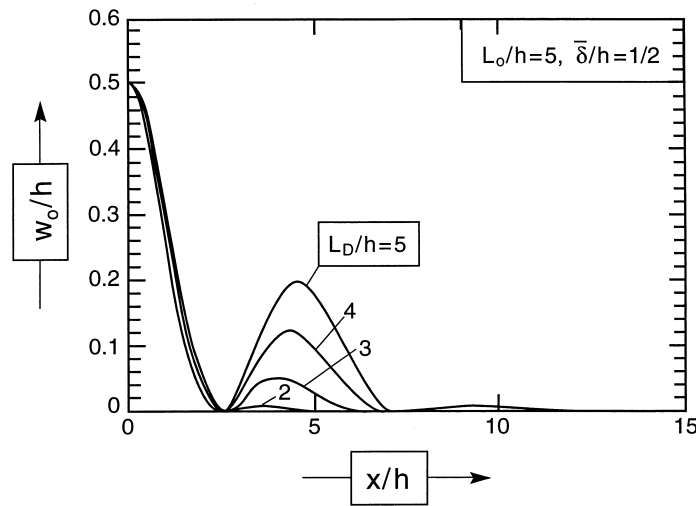


Fig. 7. The shapes of the extended imperfection used in the analysis.

implemented in the nonlinear mode with updated geometry and employing eight-noded axisymmetric elements with five to ten elements through the thickness. For the small imperfection cases, most computations were carried out using a finite element mesh to represent the substrate. For larger detachments, most examples were run taking the attached portions of the film to be rigidly supported along the bottom surface. In general, there was little difference in the predictions obtained from these two ways of supporting the film.

3. Initial buckling

3.1. Asymptotic behavior at small imperfections

The influence of imperfections on initial buckling, expressed in terms of the induced energy release rates, are examined in order to assess the imperfection-sensitivity. This is done by imposing the initial condition that the separations be large enough to satisfy buckling in an imperfection-free film, $L=L_b$. Analytical results are provided for plane strain delaminations as well as numerical results for axisymmetric imperfections. The analytical results are asymptotically valid at small imperfection amplitudes. They are based on Koiter's asymptotic theory of post-buckling and imperfection-sensitivity for elastic structures (Koiter, 1945). A more extensive study of the role of small imperfections on buckling delamination has been conducted by Storåkers and Nilsson (1993), and thus only the outcome of the analysis will be presented here.

For $L=L_b$ the buckling mode from Eq. (4) with $w_0=0$ is

$$w = (b/2)[1 + \cos(2\pi x/L)], \quad |x| \leq L/2 \quad (15)$$

where b is the buckling deflection amplitude. For sufficiently small imperfections, the deflection of the film above the separation satisfies:

$$\frac{b}{h} = \frac{\sigma}{\sigma_0 - \sigma} k \quad (16)$$

with

$$k = 8 \int_0^{L/2} (w_0/h) \cos(2\pi x/L) dx$$

being a function of δ/h and L_0/L . Moreover, in Eq. (8) the term w'^2 is large compared to $w_0'w'$ when δ/h is small such that

$$1 - \sigma/\sigma_0 = 3(b/h)^2/4 \quad (17)$$

The preceding two equations can be solved for b and σ/σ_0 in terms of k . For sufficiently small δ/h , the asymptotic relations are

$$b/h = (4k/3)^{1/3} \quad \text{and} \quad 1 - \sigma/\sigma_0 = (\sqrt{3}k/2)^{2/3} \tag{18}$$

The limiting relation for the energy release rate from Eq. (13) is

$$G/G_0 = 3(4k/3)^{2/3} \tag{19}$$

where G_0 is given by Eq. (2).

Because k is proportional to the imperfection amplitude δ , Eq. (19) dictates that, when the imperfections are sufficiently small, the energy release rate scales as; $G \sim \delta^{2/3}$. The 2/3 power law magnifies the effect of small imperfections, producing an unusually large increase in G . Moreover, in the special case where the imperfection is in the shape of the buckling mode with $L = L_0 = L_b$, $k = \delta/h$, revealing that small imperfections have an exceptionally large influence. It must again be noted that the asymptotic result, Eq. (19), is limited to behavior in the vicinity of the onset of buckling, i.e. $L \cong L_b$.

3.2. Numerical results

The imperfection sensitivity of buckling for “large” imperfections has also been calculated, numerically, for axisymmetric buckles (Fig. 8). These results were determined for axisymmetric undulations in the same form as Eq. (11) with diameter L_0 taken to be equal to the diameter of the delamination L . Again, the notable feature is that appreciable energy release rates develop when the delamination diameter is a fraction of the diameter for the onset of buckling for

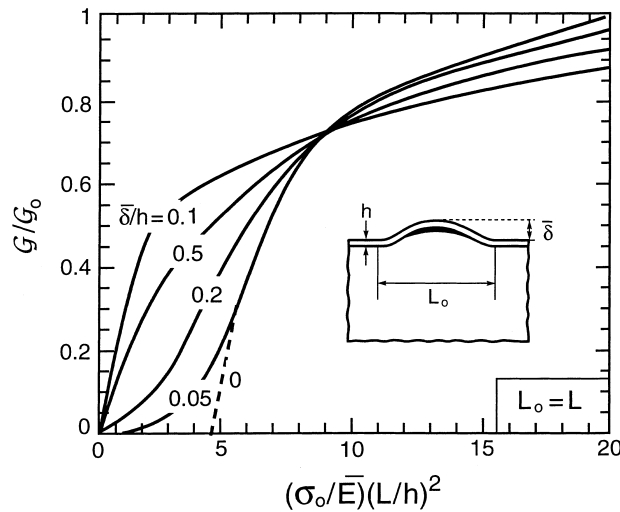


Fig. 8. The imperfection sensitivity of the energy release rate in the presence of an axisymmetric imperfection undulation whose diameter is equal to the diameter of the separation. Note the significant elevation of the energy release rate at separation diameters which are much smaller than onset of buckling for the perfect system (i.e. $(\sigma_0/\bar{E})(L/h)^2 = 4.89$).

the perfectly flat film, as has also been documented by Storåkers and Nilsson (1993). For example, when the imperfection amplitude is only, $\delta/h = 1$, a significant energy release rate develops even at delamination diameters which are only 1/3 the onset value.

4. Buckle propagation

4.1. Single wave imperfections

To highlight the strong nonlinear coupling between relatively small size imperfections and buckling delaminations, results will first be presented for *decoupled imperfection driven and buckle driven delamination* in plane strain. The buckling mode is given by Eq. (15).

An example, presented in Fig. 9, illustrates the behavior. It applies to the following set of parameters:

$$\frac{\sigma_0}{E} = 0.005 \left(\frac{L_b}{h} = 25.7 \right), \quad \frac{L_0}{h} = 5 \left(\frac{L_0}{L_b} = 0.195 \right), \quad \bar{E}_s = \bar{E}(\alpha_D = 0)$$

To decouple the two effects, first the imperfection is taken to be zero for buckling delamination, and thereafter, for the imperfection driven delamination, the

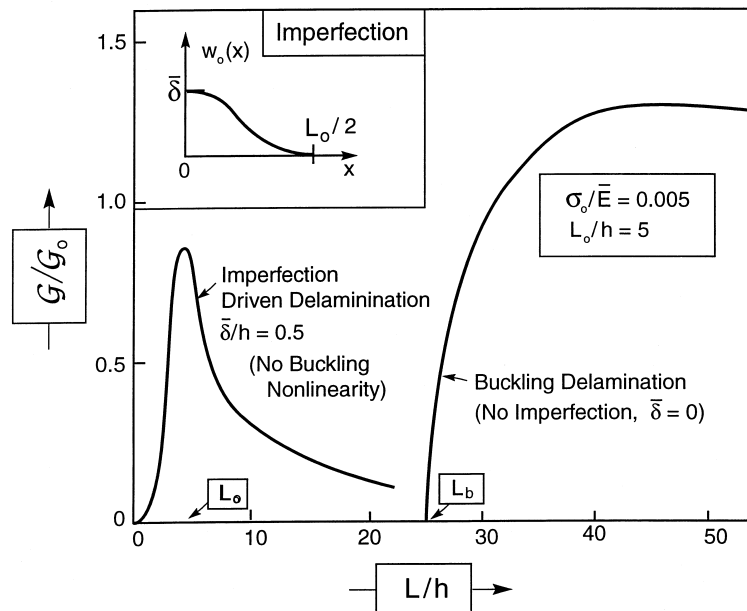


Fig. 9. Decoupled energy release rates associated with nucleation and buckle-driven delamination at plane strain undulations.

nonlinear deflections are deleted. When this is done (Fig. 9), it is found that, when the wavelength of the imperfection, L_0 , is small compared with the onset buckling wavelength, L_b ($L_0/L_b = 0.195$), there is little overlap in the energy release, with G dropping to a small value well before the delamination is large enough to be driven by buckling. These decoupled results affirm that there exists a major barrier impeding propagation of the delamination much beyond the width of the imperfection itself.

The coupled results determined with the full nonlinear equations (Fig. 10a and b), indicates a very different picture, similar to that anticipated on Fig. 5. Now, while the energy release rate decreases as the delamination spreads beyond the imperfection, it begins to increase again well before its length attains L_b . As already noted (Section 3), the influence of the imperfection is particularly dramatic for separation widths $L \approx L_b$, even though the imperfection width is less than $L_b/5$.

The mode mixity ψ at the right hand tip of the interface delamination is plotted in Fig. 11. There is significant variation in ψ depending on both imperfection level and delamination width. This variation exerts an important influence on the spread of the delamination. Note that sufficiently wide buckling-driven delaminations always approach mode II conditions (at $L/h \approx 60$ in this example). The relative proportion of mode II is less for delaminations with curved fronts. For this reason, delaminations tend to arrest at a characteristic width and then continue spreading along their front (Hutchinson and Suo, 1992).

The strong interaction of the two types of delamination with disparate wavelengths is a consequence of nonlinear coupling. In Fig. 10a the imperfection width is only about one fifth the width of the onset buckle, yet there is strong coupling, such that G_{\min} is well above zero. For a somewhat longer imperfection, but still short compared to L_b (Fig. 10b), the peak is about the same, but the minimum is even larger. Accordingly, nucleation conditions are similar, but propagation is facilitated.

To elaborate on nucleation and the barrier to propagation, plots of G_{peak}/G_0 and G_{\min}/G_0 in plane strain are presented in Fig. 12, as a function of L_0/L_b , for two imperfection amplitudes. *Presented this way, the results are independent of σ_0/\bar{E} , as shown in Appendix A.* This feature suggests introduction of another non-dimensional index, referred to as the imperfection size index, \mathcal{R} . It is given by:

$$\begin{aligned} \mathcal{R} &= (L_0/L_b)^2 = 0.305(\sigma_0/\bar{E})(L_0/h)^2 \text{ (plane strain)} \\ &= 0.204(\sigma_0/\bar{E})(L_0/h)^2 \text{ (axisymmetric)} \end{aligned} \tag{20}$$

The general form of the minimum is:

$$G_{\min} / G_0 = F[L_0/L_b, \bar{\delta}/h] \tag{21}$$

where F is a function which could be obtained by fitting to Fig. 12. Note, however, that the dependence on L_0/L_b is essentially linear and the dependence on

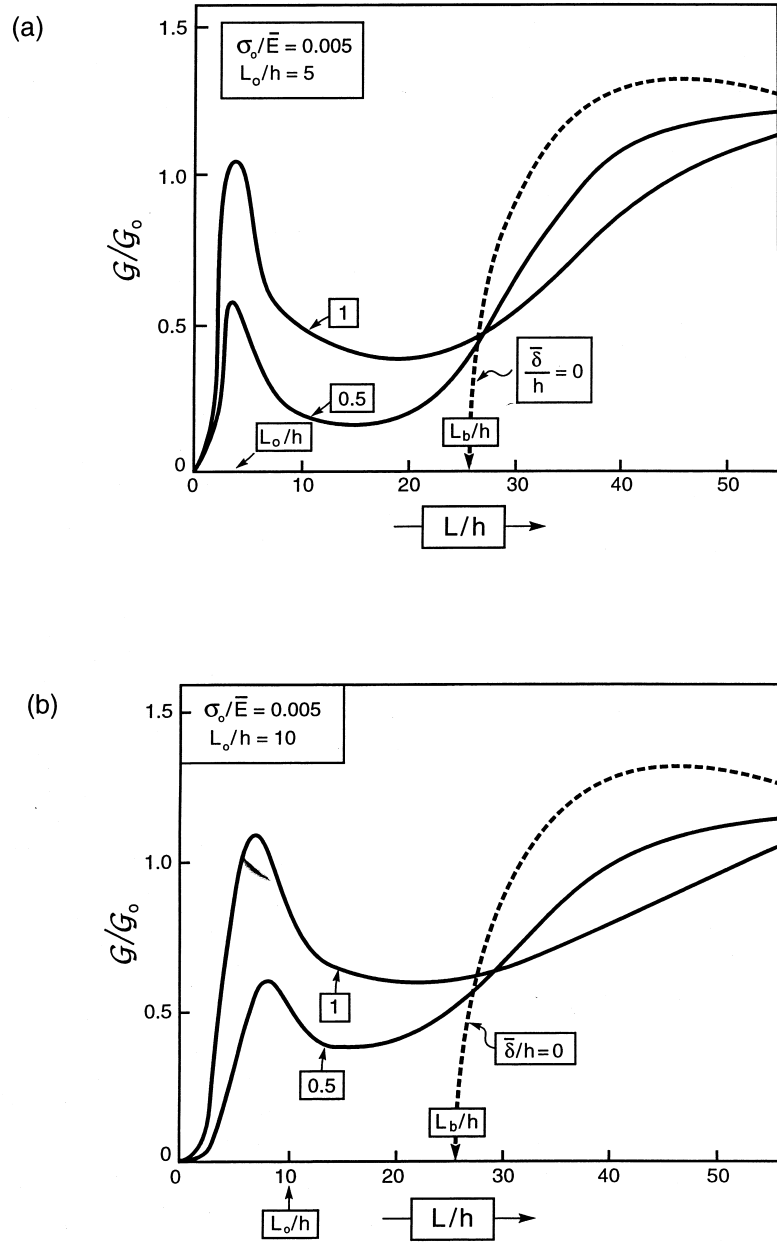


Fig. 10. Energy release rates for plane strain undulations demonstrating the coupling between small imperfections and large buckling deflections: (a) $L_0/L_b = 0.195$ (b) $L_0/L_b = 0.39$.

δ/h is weak: features also found below for axisymmetric imperfections. Consequently, Eq. (21) can be approximated by:

$$G_{\min} / G_0 \cong c(L_0/L_b) \tag{22}$$

where c is in the range 0.8 to 1.0 (Fig. 12) for imperfections amplitudes in the range $0.5 < \delta/h < 1$. This result and its axisymmetric analog are used in Section 5 to evaluate a critical imperfection wavelength for buckle propagation.

4.2. Extended imperfections

Extended oscillatory interface imperfections can trap a nascent delamination in regions where w_0'' is positive. The family of imperfections plotted in Fig. 7 provides an illustration of this effect. The nominal width of each undulation is taken to be $L_0/h = 5$. Numerical results for the energy release rate are shown in Fig. 13 as a function of the delamination width, for four imperfection shapes. The peak, G_{peak} , is insensitive to the decay length, L_D , but the minimum, G_{min} , is a strong function of L_D . For $L_D/h = 2$, the behavior is similar to that shown in Fig. 10a for the single imperfection having the same amplitude ($\delta/h = 1/2$). However, at larger L_D/h , trapping becomes a dominant feature, resulting in low G_{min} . An imperfection with $L_D/h = 5$ results in $G_{\text{min}}/G_{\text{peak}} \approx 1/10$.

Two-dimensional variations of the surface imperfections may well provide opportunities for the delaminations to spread around such “traps”. Nevertheless,

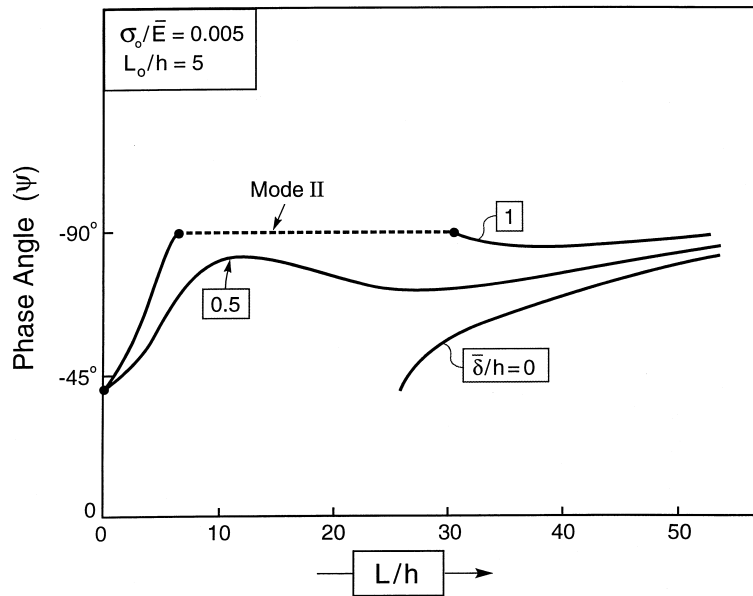


Fig. 11. Variation in mode mixity angle with separation length for a plane strain buckle.

the limited one-dimensional study presented here indicates that the nonlinear coupling between small imperfection-driven delaminations and the larger buckling-driven delaminations depends on details of the imperfection shape. The strong coupling can be defeated by undulations which trap the delaminations while they are still small.

4.3. Axisymmetric imperfections

Energy release rate results for axisymmetric undulations have been obtained numerically for a range of undulation wavelengths and amplitudes. Typical results are presented on Fig. 14 for a range of the imperfection size index, Eq. (20) between 0.12 and 0.6. The features anticipated schematically on Fig. 5 are again apparent.

The analytical results assert that when L_0/L_b is used as the abscissa, G_{\min}/G_0 should be independent of the residual strain, σ_0/\bar{E}_f . This dependence is

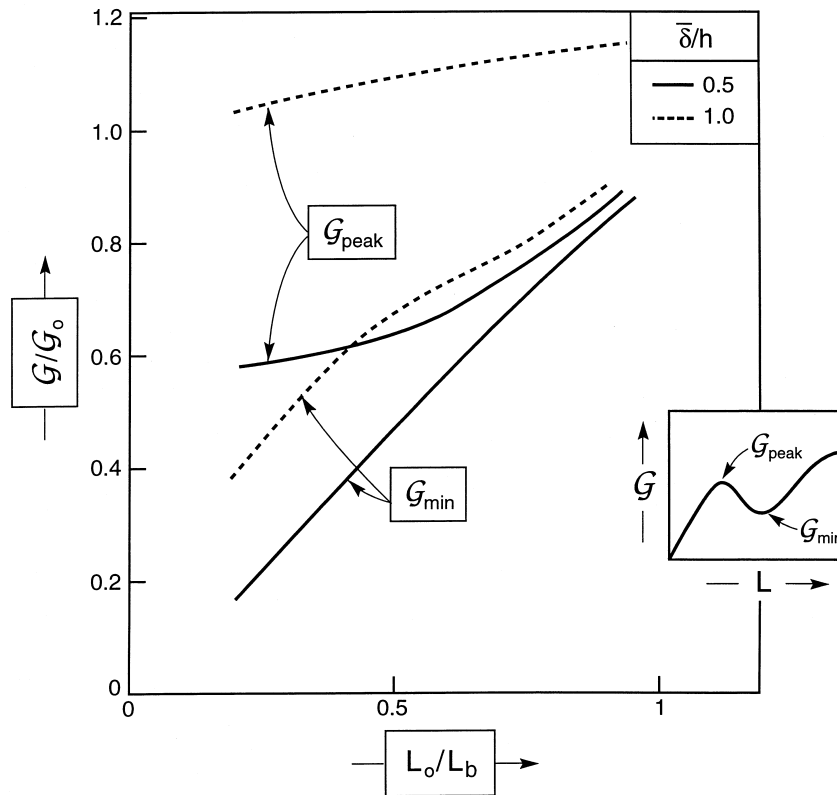


Fig. 12. Non-dimensional plots illustrating the dependence of the peak and minimum energy release rates in plane strain on the relative undulation wavelength L_0/L_b .

demonstrated on Fig. 15a. A fit to these results in the range $0.5 < L_0/L_b < 1$ has the same form found for plane strain delaminations, Eq. (22):

$$G_{\min} / G_0 \cong c(L_0/L_b) \tag{23}$$

where now $c \cong 0.4$. Note that there is minimal effect of the undulation amplitude, even less than that for plane strain delamination (Fig. 12).

5. Critical conditions

5.1. Buckle propagation

Upon equating G_{\min} to the interface fracture toughness at the associated mode mixity, Γ_i , Eqs. (22) and (23) indicate that there is a critical imperfection wavelength, $L_0^c \equiv L_0$, given by:

$$L_0^c = [\Gamma_i L_b / (cG_0)]$$

$$\cong 4 \left(\frac{\bar{E}\Gamma_i}{\sigma_0^2} \right) \sqrt{\frac{\bar{E}}{\sigma_0}} \text{ (plane strain)}$$

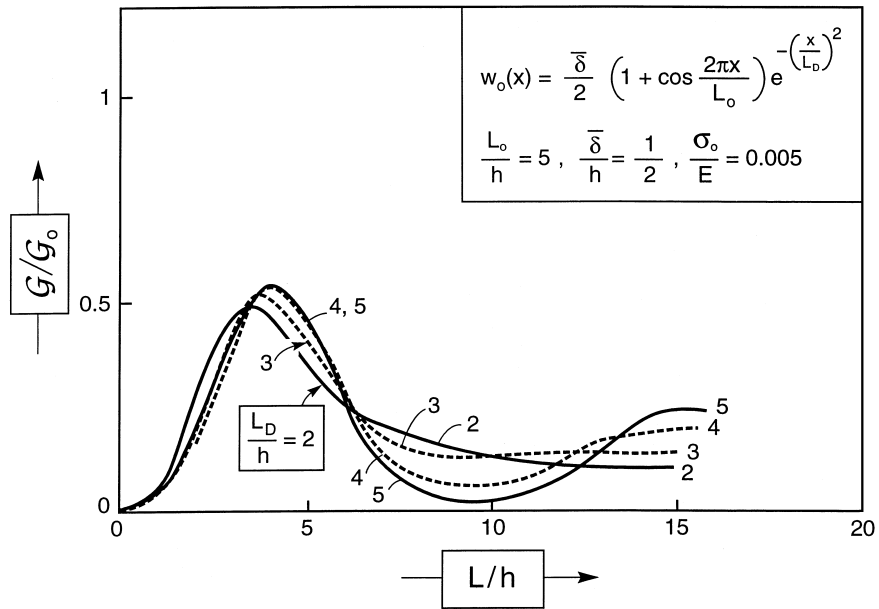


Fig. 13. Influence of extended imperfections on the energy release rate in plane strain.

$$\mathcal{R} \approx 11 \left(\frac{\bar{E}\Gamma_i}{\sigma_0^2} \right) \sqrt{\frac{\bar{E}}{\sigma_0}} \quad (\text{axisymmetric}) \quad (24)$$

Note that L_0^c is insensitive to the film thickness, h , and imperfection amplitude, δ , for the range $0.5 < \delta/h$.

The significance of this result is as follows. *Imperfections having wavelength L_0 smaller than L_0^c will not give rise to energy release rates large enough to attain a buckled state.* Accordingly, such imperfections cannot cause failure. Conversely, imperfections having larger wavelength could buckle and cause failure, subject to the presence of a defect large enough to nucleate a separation.

A paradox with Eq. (24) envisaged as a sole failure criterion is that it has no dependence on the film thickness, inconsistent with practical experience (Wright, 1998). The film thickness enters when a nucleation criterion is also imposed, based on G_{peak} , discussed next. Both *criteria* must be satisfied to cause failure.

5.2. Nucleation

In crack nucleation problems in brittle systems (notably those for cracking at indentations and inclusions) (Marshall et al., 1982; Rühle et al., 1987; Shum and Huang, 1990; Green, 1982; Ito et al., 1981; Evans, 1972), the correct scaling is

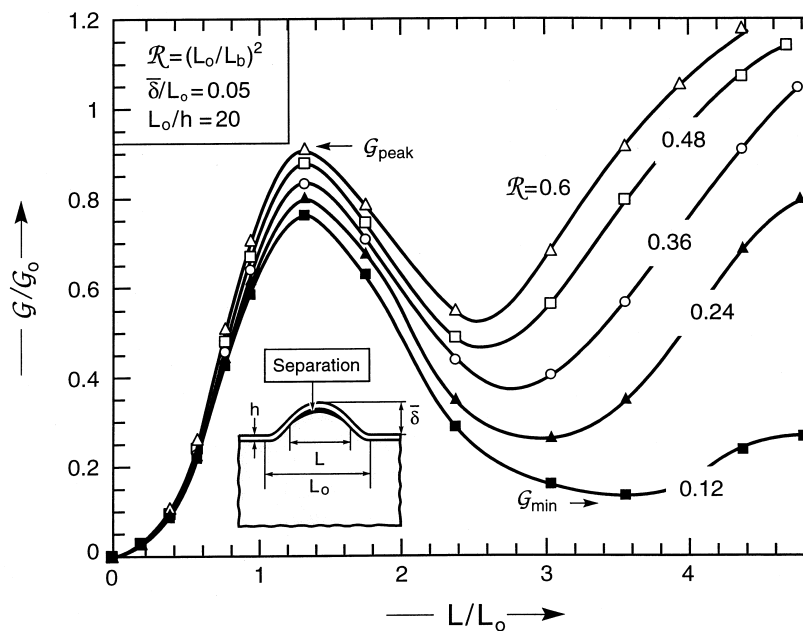


Fig. 14. Energy release rates calculated for axisymmetric undulations over the parameter range indicated on the inset.

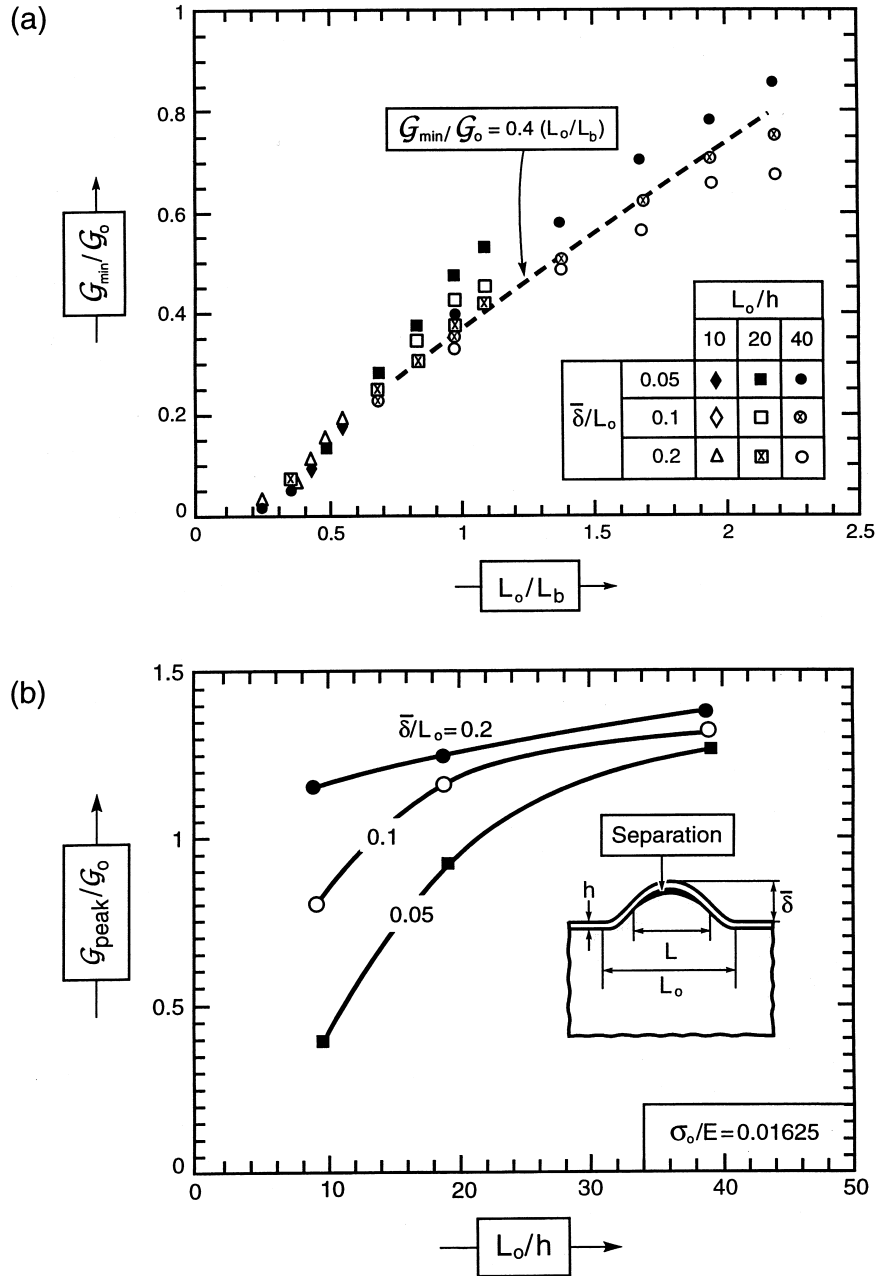


Fig. 15. Non-dimensional minimum and peak energy release rates for axisymmetric undulations, plotted as a function of imperfection index: (a) minimum, (b) peak.

achieved upon equating G_{peak} to the toughness, Γ_i . However, because of the requirement that flaws be present to activate the nucleation process, nucleation conditions must take into account representative initial flaws. This can be done approximately by equating $G_{\text{peak}}/2$ (rather than G_{peak}) with Γ_i (Green, 1982; Ito et al., 1981). In order to implement this approach in the present context, it is noted that G_{peak} for both plane strain (Fig. 12) and axial symmetry (Fig. 15b) are reasonably approximated by G_0 for moderate, but realistic, imperfection amplitudes (e.g. $\delta/h \approx 1$). Recall that G_{peak} has little dependence on the imperfection size, L_0 . Imposition of $G_{\text{peak}}/2 = \Gamma_i$ with $G_{\text{peak}} \cong G_0$ gives the critical thickness h_c at which the imperfections nucleate delaminations:

$$h_c \cong 4\bar{E}\Gamma_i/\sigma_0^2 \quad (25)$$

This result depends weakly on L_0/h and only requires modest undulation amplitudes. Note that, from Eq. (24), L_0^c and h_c are inter-related by

$$\begin{aligned} L_0^c/h_c &\cong \sqrt{\bar{E}/\sigma_0} \text{ (plane strain)} \\ &\cong 2.7\sqrt{\bar{E}/\sigma_0} \text{ (axisymmetric)} \end{aligned} \quad (26)$$

For smaller imperfections than those assumed, h_c will be larger than Eq. (25). It can be obtained from the curves presented on Figs. 12 and 15b, with Eq. (26) modified accordingly.

The following interpretation should be given to the two critical lengths. The combined inequalities $h < h_c$ and $L_0 < L_0^c$ comprise a *fail-safe condition*. Film thicknesses less than critical will not nucleate initial delaminations. Moreover, even if initial delaminations develop equal in size to the undulations (L_0), they will arrest before they become unstable. Conversely, if both inequalities are reversed ($h > h_c$ and $L_0 > L_0^c$), delaminations would be expected to nucleate and grow unstably, except that interfaces having high perfection (no defects) would still be capable of resisting failure.

6. Implications

6.1. Revised buckling map

The influence of the imperfections on film failure can be visualized by modifying the buckling map of Fig. 3 to include the energy release rate features found in the nucleation phase. Such a map of $\Sigma \equiv \sigma_0[(1-\nu^2)h/(2E\Gamma_i)]^{1/2}$ vs L/L_b is shown schematically in Fig. 16. The consequences for film failure are illustrated by the trajectory superposed on the buckling map. Present an initial interface defect, size L_0 , a critical level is reached (position A) at which a separation pops in to a stable size (position B). As Σ further increases, the separation expands

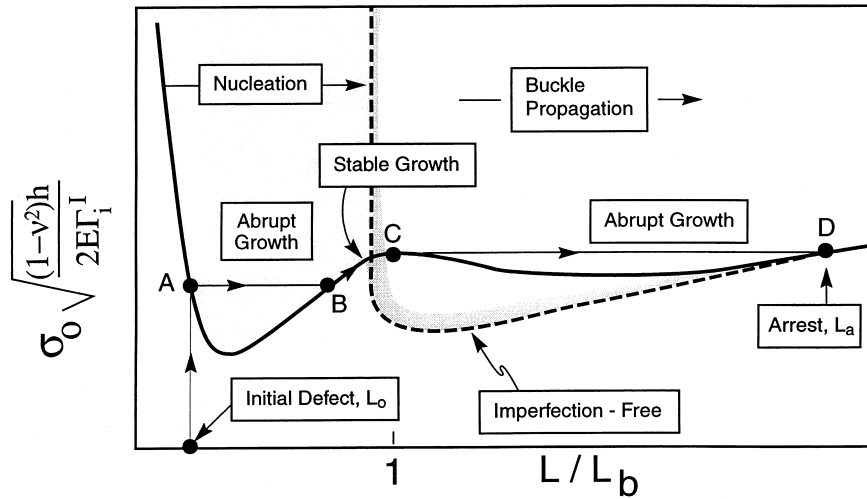


Fig. 16. A modified buckling map that introduces a nucleation condition. The trajectories are described in the text.

stably up to the maximum (point C). Here the separation buckles and abruptly expands to size L_a (point D). At this stage, the buckle may either spall or arrest, depending on conditions relative to the spall criterion (Hutchinson and Suo, 1992; Wang and Evans, 2000). If it arrests, it can again expand stably as Σ increases until spalling conditions are reached. The preceding energy release rate results can be used to plot explicit buckling maps, as a function of imperfection size and shape.

6.2. Critical sizes

Explicit failure conditions are found by determining the critical sizes, L_0^c and h_c . They are illustrated for a thin thermally grown $\alpha\text{-Al}_2\text{O}_3$ (TGO) on a superalloy. The film properties are quite well known (Table 1). The residual compression is

Table 1
Properties of $\alpha\text{-Al}_2\text{O}_3$ thermally grown on Ni-based bond coats

E (GPa)	380–400
ν	0.2
α ($^{\circ}\text{C}^{-1}$) (ppm)	7–8
α_s ($^{\circ}\text{C}^{-1}$) (ppm) ^a	14–16
h (μm)	1–10
Γ_i^0 (J m^{-2})	5–20
ΔT ($^{\circ}\text{C}$)	1000
λ	0.1–0.3

^a Ni based superalloy.

about $\sigma_0 \approx 3$ GPa, while Γ_i varies from the low end of the range (5 J m^{-2}) to an upper level given by the TGO itself ($\Gamma_0 \approx 20 \text{ J m}^{-2}$).

For axisymmetric undulations, neglecting mode mixity effects, the critical imperfection wavelength L_0^c needed to assure propagation and buckling ranges from 20 to 100 μm ; while the corresponding critical TGO thickness required for nucleation, h_c , varies from 1/2 to 3 μm . Note that the ratio $L_0^c/h_c \approx 30$ is large enough to allow application of Eq. (26), provided that the amplitude, $\delta/L > 0.05$. Undulations having such magnitude are readily developed by wrinkling, etc. (Tolpygo and Clarke, 1998). Hence, for this thin film system, imperfections comprising locally undulating surfaces provide an effective means for nucleating and propagating failure whenever the TGO thickness exceeds 1/2–3 μm . Further definition is dependent on specifics regarding the interface toughness.

When mode mixity effects are included, h_c increases significantly, dependent on λ , Eq. (6). Upon using the λ measured for TGO (0.3) (Wang and Evans, 1998) in conjunction with ψ calculated on Fig. 11, there is a factor 4 increase: such that L_0^c now ranges from 80 to 400 μm .

7. Summary

Analysis of prototypical imperfections associated with thin compressed films has established criteria for failure by buckle driven delamination. Two basic requirements must be satisfied. One based on the nucleation of interface separations. The other governed by buckling and buckle propagation.

For sufficiently large imperfections, these requirements can be expressed in terms of “critical sizes”, manifest as a critical film thickness h_c , and a critical undulation wavelength, L_0^c . Values for these critical sizes determined for a thin thermally grown oxide (TGO), have provided information that can be compared with experimental findings. Analogous results for other imperfections, such as heterogeneities, remain to be determined.

Acknowledgements

The work of JWH was supported in part by the NSF under grant CMS-9634632 and in part by the Division of Engineering and Applied Sciences, Harvard University. The work of MYH was supported in part by the Advanced Gas Turbine Systems Research program of the Department of Energy under grant 98-01-SR068 through the South Carolina Energy Research and Development Center. The work of AGE was supported by the Office of Naval Research.

Appendix A. The plane strain model

Eq. (4) can be put in the following dimensionless form:

$$W'' + (2\pi\xi)^2 W = -(2\pi\xi)^2 W_0 + m \tag{A1}$$

$$\xi^2 = 1 - \frac{3}{\eta\pi^2} \int_0^{\eta/2} [W'^2 + 2W_0 W'] dX \tag{A2}$$

where

$$\xi^2 = \frac{\sigma}{\sigma_0}, \quad \eta = \frac{L}{L_b}, \quad L_b = \pi \sqrt{\frac{\bar{E}}{3\sigma_0}} h, \quad X = \frac{x}{L_b}, \quad (\cdot)' = \frac{d(\cdot)}{dX}, \tag{A3}$$

$$W = \frac{w}{h}, \quad W_0 = \frac{w_0}{h}$$

As defined in Eq. (5), L_b is the width of the delamination associated with the onset of buckling in the perfect film. The constant $m = 4\pi^2 M^A / (\sigma_0 h^2)$ is one of the free variables required to meet the two boundary conditions: $W = W' = 0$ at $X = \eta/2$.

Solutions to Eq. (A1) for symmetric imperfections are given by

$$W(X) = A \cos(2\pi\xi X) + \frac{m}{(2\pi\xi)^2} - F(X, \xi) \tag{A4}$$

where A is an undetermined coefficient and

$$F(X, \xi) = (2\pi\xi)^2 \cos(2\pi\xi X) \int_0^X \left[\frac{1}{\cos(2\pi\xi\phi)^2} \int_0^\phi \cos(2\pi\xi X') W_0(X') dX' \right] d\phi \tag{A5}$$

Enforcement of the boundary conditions gives

$$m = \frac{2\pi\xi F'(\eta/2, \xi)}{\tan(\pi\xi\eta)} + (2\pi\xi)^2 F(\eta/2, \xi), \quad A = -\frac{F'(\eta/2, \xi)}{2\pi\xi \sin(\pi\xi\eta)} \tag{A6}$$

where $F' = dF/dX$. By Eq. (A4),

$$W'(X) = -F'(X, \xi) + F'(\eta/2, \xi) \sin(2\pi\xi X) / \sin(\pi\xi\eta) \tag{A7}$$

The use of Eq. (A7) in Eq. (A2) gives a single equation for ξ in terms of η . Note that this relation *depends only on the dimensionless parameters specifying the imperfection*. Generally, ξ must be determined numerically. The solution is then fully determined from Eq. (A7) and the other equations.

For the imperfection shape of Eq. (11), the two integrations defining $F(X, \xi)$ can be carried out explicitly. The dimensionless imperfection parameters are δ/h and L_0/L_b . It is readily established that G/G_0 and ψ depend only on η , δ/h and L_0/L_b .

References

- Christensen, R.J., Tolpygo, V.K., Clarke, D.R., 1997. The influence of the reactive element yttrium on the stress in alumina scales formed by oxidation. *Acta Mater.* 45, 1761–1766.
- Evans, A.G., 1972. The strength of brittle materials containing second phase dispersions. *Phil. Mag.* 26, 1327.
- Evans, A.G., Hutchinson, J.W., 1995. The thermomechanical integrity of thin films and multilayers. *Acta Metall. Mater.* 43, 2507–2530.
- Evans, A.G., He, M.Y., Hutchinson, J.W., 1998. Effect of interface undulations on the thermal fatigue of thin films and scales on metal substrates. *Acta Mater.* 45, 3543–3554.
- Gioia, G., Ortiz, M., 1997. Delamination of compressed thin films. *Adv. Appl. Mech.* 33, 120–192.
- Green, D.J., 1982. Critical microstructures for microcracking in Al_2O_3 - ZrO_2 composites. *J. Am. Ceram. Soc.* 65, 610–614.
- He, M.Y., Evans, A.G., Hutchinson, J.W., 1998. Effects of morphology on the decohesion of compressed thin films. *Mat. Sci. Eng. A245*, 168–181.
- Hutchinson, J.W., Suo, Z., 1992. Mixed mode cracking in layered materials. *Adv. Appl. Mech.* 29, 63–191.
- Hutchinson, J.W., Thouless, M.D., Liniger, E.G., 1992. Growth and configurational stability of circular, buckling-driven film delaminations. *Acta Metall. Mater.* 40, 295–308.
- Ito, Y.M., Rosenblatt, M., Cheng, L.Y., Lange, F.F., Evans, A.G., 1981. Cracking in particulate composites due to thermalmechanical stress. *Intl. J. Frac.* 17, 483–491.
- Koiter, W.T., 1945. On the stability of elastic equilibrium, thesis Delft (in Dutch with English summary). H. J. Paris, Amsterdam.
- Koiter, W.T., 1966. On the nonlinear theory of thin elastic shells. *Proc. Kon Ned. Ak. Wet.* B69, 1–54.
- Marshall, D.B., Lawn, B.R., Evans, A.G., 1982. Elastic/plastic indentation damage in ceramics: the lateral crack system. *J. Am. Ceram. Soc.* 65, 561–566.
- Nilsson, K.F., Giannakopoulos, A.E., 1995. A finite element analysis of configurational stability and finite growth of buckling driven delamination. *J. Mech. Phys. Solids* 43, 1983–2021.
- Rühle, M., Evans, A.G., McMeeking, R.M., Charalambides, P.G., Hutchinson, J.W., 1987. Microcrack toughening in alumina/zirconia. *Acta Metall.* 35, 2701–2710.
- Shum, D.K.M., Huang, Y.Y., 1990. Fundamental solutions for microcracking induced by residual stress. *Engnr. Fract. Mech.* 37, 107–117.
- Storåkers, B., Nilsson, K.F., 1993. Imperfection sensitivity at delamination buckling and growth. *Int. J. Solids Structures* 30, 1057–1074.
- Thouless, M.D., Jensen, H.M., Liniger, E.G., 1994. Delamination from edge flaws. *Proc. Royal Soc. London A447*, 271–279.
- Tolpygo, V.K., Clarke, D.R., 1998. Wrinkling of α -alumina films grown by thermal oxidation — II: oxide separation and failure. *Acta Mater.* 46, 5167–5174.
- Wang, J-S., Evans, A.G., 1998. Measurement and analysis of buckling and buckle propagation in compressed oxide layers on superally substrates. *Acta Mater.* 46, 4993–5505.
- Wang, J.S., Evans, A.G., 2000. Effects of strain cycling on buckling, cracking and spalling of a thermally grown alumina on a nickel-based bond coat. *Acta Mater.* (in press).
- Wright, P.K., 1998. Influence of cyclic strain on life of a PVD TBC. *Mat. Sci. Eng. A245*, 191–200.